Journal of Statistical Physics, Vol. 112, Nos. 1/2, July 2003 (© 2003)

A Markov Model for Kinesin

Christian Maes[1] **and Maarten H. van Wieren**[1]

Received July 17, 2002; accepted February 5, 2003

We investigate the validity of a Markov approach for the motility of kinesin. We show in detail how the various mechanochemical states and reaction rates that are experimentally measured, can be used to create a Markov-chain model. We compare the performance of this model to motility data and we find global similarities in the load and ATP-concentration dependency of speed and mean run length. We also discuss the relation between the experimentally found stalling behavior and thermodynamic expectations. Finally, the Markov chain modelling provides a way to calculate the mean entropy production and the (power) efficiency.

KEY WORDS: Biochemical processes; molecular motors; kinesin.

1. INTRODUCTION

Molecular motor is a common name for a variety of mechanisms whereby on a molecular scale chemical energy is transformed into work. Most often they consist of complex enzymes taking care of transport and motion in living cells. The detailed dynamics of molecular motors has not been fully understood and since many years the problem has also fascinated physicists. To activate kinesin a strong nonequilibrium is maintained via a high concentration of one of the reactants, ATP (adenosine triphosphate), a common biological energy source. Its hydrolysis $ATP \leftrightarrows ADP + P_i$ into adenosine diphosphate and inorganic phosphate produces the energy for the molecular motor. In the present paper biochemical data are used to define mechanochemical states and to derive a Markov chain that models

[1] Instituut voor Theoretische Fysica, K.U. leuven, Celestijnenlaan 200D, B-3001 Leuven, Belgium; e-mail: Maarten.vanWieren@fys.kuleuven.ac.be

0022-4715/03/0700-0329/0 © 2003 Plenum Publishing Corporation

the kinesin motor. The use of Markov chains in that context is not new; a recent reference along that line is ref. 1. Here however, the Markov model is not only a framework to fit the experimental results but the states and transition rates for the Markov approximation are obtained in a step by step process from combining biochemical knowledge with the standard procedures of statistical physics. A similar ambition gave rise in ref. 2 to a phenomenological model of dynamical equations for the mechanical cycle in kinesin. The experimental input comes from refs. 3 and 4. We find that the theoretical model behaves well with respect to most experimental results. In particular we regard the stalling behavior and address the question why the experimentally found stall force seems to be in discordance with a thermodynamic argument that suggests a linear dependence of the stall load on the chemical potential difference (i.e., the logarithm of the ATP concentration). We also investigate for the first time the entropy production and, related to that, the efficiency within such a detailed Markov model. This is interesting in the light of recent theoretical studies in nonequilibrium statistical mechanics where the very definition of entropy production was discussed and where a symmetry was discovered in the fluctuations of the entropy production rate, see, e.g., ref. 5 also for additional references. The experimental verification of such a symmetry for small scale systems was recently reported in ref. 6 but no data are available for molecular motors. The wider context of our investigations is the thermodynamics of small (sub)systems which is a rapidly growing arena for tackling many problems in the life sciences and in manufacturing, see for instance ref. 7.

1.1. Kinesin

The protein kinesin is called a motor enzyme or a molecular motor because it is capable of linear transport along microtubules. A kinesin molecule is about 110 nm long and 10 nm thick and consists of two heads (the reactive core of the molecule) connected to two interwoven strands. On the other end of these strands a variety of cargo may be carried (e.g., packages with chemical constituents or chromosomes). Experimentally, one can *in vitro* apply a load to this end pulling it back. The two heads are the motor domains that interact alternately with the microtubule to generate movement. Studies[8,9] show that the head in front tugs the head in the back forward. This tugging, the so-called "power-stroke," is initiated by association of the head in front with an ATP-molecule. One imagines that the motor contains a pre-strung spring that is unstrung as a result of the binding of an ATP molecule; together with asymmetries in the binding to the microtubule this drives the motor forward. In the next step the ATP is

hydrolyzed into ADP and P_i. With this reaction the relevant head gains energy (about 20 kT or 83×10^{-21} J)[10] that causes a return into its original pre-strung state -after the release of the P_i and ADP. The number of ATP molecules hydrolyzed per mechanical step remains 1/1 for a broad range of loads.[11] In the mean time the head that was tugged forward binds to the microtubule under dissociation of the ADP molecule that was still present in its reaction core. The enzyme has now moved one step (of about 8.1 nm, refs. 11 and 12). The other head can then release its P_i and becomes loosely bound to the microtubule, thereby completing the reaction cycle. We will come back to the details of this cycle in Section 3. It should be mentioned that this alternating head-over-head motion of kinesin has been challenged by the experiments of ref. 13.

1.2. Outline of the Paper

Chemical kinetic descriptions go back to some ten years ago, see, e.g., ref. 14 whereas ratchet models are more recent, see, e.g., refs. 15–17. While these diffusion (or thermal) ratchets have certainly brought new ideas and simple toy-models have demystified certain basic mechanisms, the correspondence with the bio-chemical reality has not been impressive. Markov chain modelling of kinesin motility with discrete states has appeared before in, e.g., refs. 1, 18, and 19 with various choices for the states yielding largely improved results. The experimental results of refs. 3 and 4 are very well reproduced there by fitting the proposed theoretical models. In the present paper we report further progress in mainly two directions: (1) to motivate in detail the specifications of the Markov chain modelling where the states and transitions are taken as closely as possible to the biochemical facts; (2) to enlarge the domain of study to include also considerations on entropy production.

We start in the next section with some preliminaries concerning setting up the Markov model and its possible relevance to mechanochemical evolutions. In Section 3 we describe our reduction of the complexity of the kinesin motility to a Markov chain model. For this we need to identify the relevant state space and we need to estimate the transition rates between the possible states. These steps are highly non-trivial. On the one hand we require a specific form for the rates based on a general statistical mechanical principle; on the other hand there is the work of fitting and estimating remaining parameters. Finally, in Section 4, we evaluate to what extent the model reproduces known biological data, concentrating on aspects of velocity, efficiency and entropy production and how they depend on ATP concentration and load.

2. MARKOV APPROXIMATION

2.1. Chemical Motor Model

The molecular motor kinesin works, through its mechanical couplings, on the energy release in the dissociation of ATP. We make here some abstraction of the actual processes to obtain a simple thermodynamic scheme of a chemical motor.

Consider a system coupled to two particle reservoirs at chemical potentials μ_1 and μ_2, everything immersed in a bath at constant temperature and pressure. In the system the particles undergo a reaction: the simplest thing is to assume two energy levels $e_1 \geqslant e_2$ with the particles from the first particle reservoir entering the system at level e_1. The reaction takes them down to level e_2 after which they leave to the second particle reservoir. The heat per particle that is released to the thermal reservoir is denoted by Q and the work per particle that is done by the system is denoted by W. The work consists in a conformational change of the system (giving rise to motion). In the steady state, a particle current is maintained and work is done while heat is exchanged with the environment.

By energy conservation (per particle):

$$W + Q + e_2 - e_1 = 0 \tag{1}$$

For the (total) entropy production in the steady state, we must add the changes of entropy in all the reservoirs and the second law gives

$$Q + (\mu_1 - e_1) - (\mu_2 - e_2) \geqslant 0 \tag{2}$$

As a consequence, by eliminating Q, the maximal work per particle that can be done by our molecular motor is always bounded as

$$W \leqslant \mu_1 - \mu_2 \tag{3}$$

On the other hand, if $Q \geqslant 0$ (heat released to the environment), then also

$$W \leqslant e_1 - e_2 \tag{4}$$

and $Q \leqslant 0$ implies $W \geqslant e_1 - e_2$. This is all what can be said thermodynamically about the theoretical efficiency of our motor. Note that the above thermodynamics is indifferent to the smallness of the system (such as a molecular motor) as long as the reservoirs can be considered macroscopically large. For our molecular motor the particle reservoirs form the environment with which the motor exchanges ATP and its constituents. The state of the αth reservoir is a non-negative integer n_α and it gives the

number of particles of species α present in the reservoir. This reservoir is characterized by a chemical potential μ_α which is maintained throughout. The heat bath or thermal reservoir fixes the inverse temperature β^{-1}, corresponding, e.g., to body temperature, in which all other reservoirs and system are immersed. Finally the motor can do work against some external force (called load) by moving some distance related to conformational changes.

Going to the full details of the biochemical reality is too much of a task. A standard procedure is to invoke the so called Markov approximation. The evolution is given on the level of reduced states of a much more complicated microscopic process.

2.2. States and Rates

The first introductions of Markov processes in the study of chemical reactions can be found in refs. 20 and 21. In our case, not only pure chemistry but also mechanics will specify the transition rates. We follow here the line of ref. 5, Sections 5 and 6.2, specialized to a mechanochemical system.

The state of the motor is characterized by both chemical and mechanical aspects. For example the kinesin heads can be filled with ATP or their constituents and strains may exist between the heads. In general the states of the motor are characterized by numbers $x = (x_1,\ldots, x_m)$ giving each time the number of particles of species α present, and by coordinates $y = (y_1,\ldots, y_s)$ giving the mechanical description. In this way, $i = (x, y) \in \Omega$ is a reduced state for the motor and Ω will denote the (finite) state space.

We want to define a Markov process for the (x, y). The dynamics is as follows. There are exchanges of particles between the particle reservoirs and the subsystem. Secondly, there are (chemical) reactions within the subsystem by which the numbers x change (but not the n_α) and by which energy is released to the thermal reservoir. This also involves the substrate (microtubule) and the attachment of the motor to katalytic sites. Thirdly, there are the conformational transitions changing the (collective) coordinates y. This can involve internal rearrangements by which again energy is exchanged with the heat bath but also motion (the power stroke) against some external force. For all these transitions the transition rates are determined by the total change of entropy. For example, in equilibrium, for a chemical reaction by which $x \to x'$ at fixed y by which energy is exchanged with the heat bath, the rates satisfy the detailed balance condition

$$\frac{r_0(x \to x', y)}{r_0(x' \to x, y)} = \exp[-\beta \Delta G] \tag{5}$$

with ΔG the Gibbs free energy. The concentrations of the various reactants (or, the equilibrium chemical potentials) are then obtained by differentiating G with respect to the x. Stationary nonequilibrium is installed when the environment maintains a different chemical potential; the concentration of ATP can be much larger than its equilibrium value. For a particle exchange between the motor and the environment the transition rates will pick up a dependence on, e.g., the ATP concentration.

We conclude that the nonequilibrium transition rates are obtained by associating with each state $i \in \Omega$ an energy G_i and we assume the transition-rates $r(i, j)$ and $r(j, i)$ between two such states i and j to satisfy:

$$\frac{r(i, j)}{r(j, i)} = \Phi(i, j)\, e^{\beta[G_i - G_j]} \tag{6}$$

where β is the inverse temperature and $\Phi(i, j) = 1/\Phi(j, i)$ will break the detailed balance condition as a consequence of the driving mechanism via the gradient in chemical potential, possibly counteracted by some external load.

We can solve (6) by the choice

$$r(i, j) = \frac{\omega_{ij} e^{\beta \mu_{ij}}}{1 + e^{\beta[F\lambda_{ij} - U_{ij}]}} \tag{7}$$

with μ_{ij} the chemical potential of some substance α involved in the transition from state i to state j. The difference in energy is in the exponential, $F\lambda_{ij} - U_{ij}$ with $U_{ij} = G_i - G_j$, the free energy difference between state i and state j without load. $F\lambda_{ij} = \vec{F} \cdot \vec{\lambda}_{ij}$ is the product of an external load acting from state j to state i over "distance" $\vec{\lambda}_{ij} = -\vec{\lambda}_{ji}$. Since in the motility cycle the whole configuration has shifted over the stepping distance (≈ 8 nm) we demand that $\sum_{\text{cycle}} \lambda_{ij} = \lambda$.

Expression (7) is further parameterized by $\omega_{ij} = \omega_{ji}$. We call ω_{ij} the characteristic frequency of transition (i, j); it can possibly be seen as a measure of the friction of the transition and may still depend on the applied load F due to some conformational change inside the kinesin head. By the symmetry $i \leftrightarrow j$, it cannot have a definite influence on the nonequilibrium features of the motion. Comparing (7) with (6) we have

$$\Phi(i, j) = e^{-\beta[F\lambda_{ij} - \mu_{ij} + \mu_{ji}]} \tag{8}$$

and (7) solves (5) in equilibrium.

We will take the ω_{ij} constant (not dependent on the load) so that the main implication of formula (7) is that the effect of the load on the rates

is bounded by some rate-limiting process (as is the case for the whole model with respect to the ATP concentration); hence the choice of a Michaelis–Menten form in (7) seems most natural. This differs from the choices made in, e.g., refs. 1 and 18 where the rates also solve (6) but are not bounded as function of the load.

In Section 3 we will give the concrete realization of (7).

2.3. Entropy Production

The probability $\rho_t(i)$ to find the system in state i at time t satisfies the Master equation:

$$\frac{d\rho_t(i)}{dt} = \sum_{j \in \Omega} [r(j, i)\, \rho_t(j) - r(i, j)\, \rho_t(i)] \tag{9}$$

We are interested in the stationary process; that is when $\rho_t(i) = \rho(i)$ is no longer varying with time. The model describes a nonequilibrium steady state when (9) vanishes without each term in the sum being zero. We can associate a mean entropy production rate (MEP) to it, see refs. 22 and 23),

$$\text{MEP} = \sum_{i, j} \rho(i)\, r(i, j) \log \frac{r(i, j)}{r(j, i)} \tag{10}$$

MEP is always non-negative and it is zero if and only if $\rho(i)\, r(i, j) = \rho(j)\, r(j, i)$ (detailed balance).

The "current" $J_{ij}(t_1, t_2)$ over a time-interval $[t_1, t_2]$ between any two different states i and j is the random variable

$$J_{ij}(t_1, t_2) = N_{ij}(t_1, t_2) - N_{ji}(t_1, t_2) \tag{11}$$

with $N_{ij}(t_1, t_2)$ the number of transitions in $[t_1, t_2]$ from state i to state j. When sampled over a large time-interval, we get its mean, the stationary current

$$J_{ij} = \rho(i)\, r(i, j) - \rho(j)\, r(j, i) = \lim_{t \uparrow +\infty} \frac{J_{ij}(0, t)}{t} \tag{12}$$

and another way to write the entropy production rate:

$$\text{MEP} = \tfrac{1}{2} \sum_{i, j} J_{ij} A_{ij} \tag{13}$$

with $A_{ij} = \log(r(i,j)/r(j,i))$ the thermodynamic force by which the system is driven away from equilibrium. The basic relations are then

$$\sum_j J_{ij} = 0, \qquad \sum_{i,j} J_{ij} A_{ij} \geqslant 0 \tag{14}$$

and similarly to (1)–(4), they ought to decide the performance of the Markovian motor. Most interesting are the currents associated with the power stroke because from these we obtain the velocity and the possible dependence on load and ATP concentration. In the same manner, since motor functioning can hardly be imagined without a cyclic component, we are concerned with Markov chains that are at least partially cyclic. We call a Markov chain monocyclic if we can write $\Omega = \{1, 2, \ldots, n\}$ and $r(i,j) = 0$ unless $i = j \pm 1$ (with the convention that $n+1 \equiv 1$). For a monocyclic Markov chain the currents satisfy $J_{ij} = J = -J_{ji}$ when $j = i+1$ and are zero otherwise. Using (7) in (13), it is then easy to verify that the mean entropy production rate takes the explicit form

$$\mathrm{MEP} = J\beta[\Delta\mu - F\lambda] \tag{15}$$

where $\Delta\mu = \sum_{i=1}^{n} [\mu_{i,i+1} - \mu_{i+1,i}]$ and $\lambda = \sum_{i=1}^{n} \lambda_{i,i+1}$. We have taken the positive direction of the current opposite to that of the load. The power stroke is effectively generating motion (in the right direction) as long as the load $F \leqslant \Delta\mu/\lambda$, or, $\Delta\mu/\lambda$ is the maximal force that can be delivered by the motor for given nonequilibrium concentrations, see (3). It is therefore natural to say that the stall force F_{stall}, the load at which the mean entropy production vanishes, satisfies

$$F_{\mathrm{stall}} = \frac{\Delta\mu}{\lambda}. \tag{16}$$

While this monocyclic (sometimes also called linear) architecture most conveniently expresses the motion of a motor, in reality, various rate limiting steps can break the exact order of steps. Nevertheless formulae (15) and (16) remain valid if the transition rates satisfy a local detailed balance equation as in (6) with no bias or driving over internal loops except over the main motility cycle where the current is J. Consider for example the Markov chain as depicted in Fig. 2 for $n = 6$ where, in parallel, 3 linear chains connect the states 3 and 5. Again, using stationarity, if we assume that the concentration differences satisfy $\mu_{36} - \mu_{63} + \mu_{65} - \mu_{56} = \mu_{34} - \mu_{43} + \mu_{45} - \mu_{54}$ and the distances satisfy $\lambda_{34} + \lambda_{45} = \lambda_{36} + \lambda_{65}$ as would be the case without preferred direction in the subcycle of states 3, 4, 5, 6, formula (15) remains unchanged for $J = J_{12}$. The inclusion of parallel paths or

loops (as they will arise naturally from the biochemical considerations in the next section) replaces the introduction of (non-exponential) waiting times that have been used as extra fitting resources in the linear chains of ref. 1.

3. THE MODEL

Our aim is not just to find a model that fits the experimental results, but rather to continue the discussion of Section 2.2 to derive and to justify the details of a Markov chain model based on both qualitative and quantitative information about the transition rates. Only *a posteriori* will we check whether the model performs well in reproducing the experimental data. Nevertheless, some amount of fitting will be needed and this will be addressed in Section 3.3.

3.1. Reduction of States

Experiments[24] show that the P_i releases from a kinesin head prior to ADP; for one kinesin-head this leaves us with the following states: the empty head referred to as the K-state; one filled with ATP, the T-state; one filled with ADP + P_i, the P-state; and one with ADP only which is referred to as the D-state. In principle a kinesin head could in all cases be either or not bound to the microtubule. Chemical studies[24] however have shown that a kinesin head associated with ADP is unlikely to be bound to a microtubule while in the other states the kinesin head is likely to be bound to a microtubule. Therefore we take only four states per head into account; for two heads there are sixteen possible states for kinesin. These states are schematically depicted in Fig. 1 (with periodic boundary conditions), where the arrows indicate the direction of (strong) preference for the various transitions when a nonzero chemical potential difference is driving the system. All states are referred to by two capitals, the first representing the front head, the second representing the rear head.

This set of sixteen states can be further reduced on the basis of some assumptions and approximations, whereby we leave out abnormalities that arise only under extreme conditions.

We first consider the path that is generally followed by kinesin: starting from the KD-state, one head is loose and the other bound to the microtubule; by binding ATP the motor goes to the TD-state; then kinesin undergoes a transformation because of binding to the ATP-molecule, leading to the power stroke and thus to the DT-state; as a result the ATP hydrolyzes while the other head rebinds to the microtubule, thereby releasing its ADP. Since the order of these two processes is not set, kinesin can

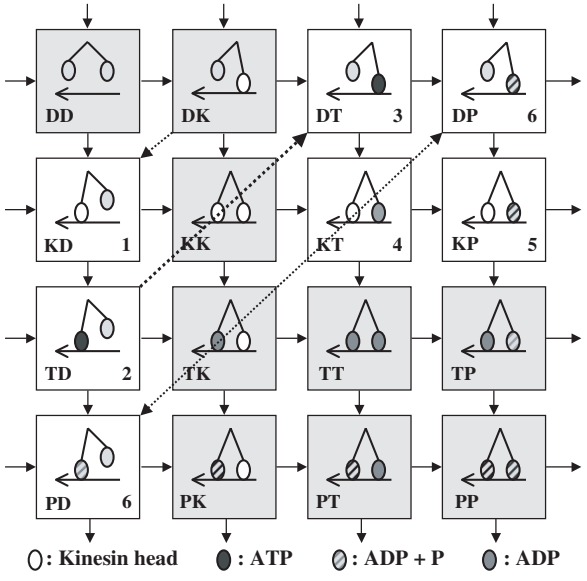

Fig. 1. Scheme of chemical states for kinesin. The arrows indicate the transitions between the states; the large dotted arrow indicates the power stroke; the grey arrows indicate the transitions that are disregarded; the grey areas indicate states that are left out of the model.

go to the KP-state via two possible ways: either through the KT-state or through the DP-state. After this so-called rate limiting step takes place, the P_i produced in hydrolysis of the ATP is released from the front head, and kinesin returns to the KD-state, the state we started with.

Sometimes kinesin may dissociate from the microtubule completely. Here we assume that this is always the case when kinesin is in the DD-state. This could happen when the head in front cannot bind to the microtubule in time and the P_i of the other head dissociates. In this model however we would like to compare to measurements for an attached motor, so we leave out this DD-state and its transitions.[2]

Fluorescence experiments[14] show that once a free kinesin molecule (in the DD-state) binds to a microtubule, it releases one of its ADP's quite quickly, but at low ATP concentrations it takes much longer to release the second ADP molecule. Because ADP release is associated with the binding of a kinesin head to the microtubule, it is clear that binding of ATP to one

[2] For considering the expected turnover rates at various microtubule concentrations, one can calculate the rate of detachment from the mean distance travelled as was measured by ref. 4 (see Section 4.5 for details) and the rate of re-attachment was measured by ref. 14.

head is needed to put the other in position to bind to the microtubule. This is confirmed by other experiments[8, 9] that show that the binding of ATP to kinesin is associated with a deformation of the head leading to a tugging force on the rear head. Altogether it seems realistic to assume that at reasonable ATP concentrations ($> 1\ \mu M$) it is unfavorable for the kinesin to release ADP from the rear head. The states associated with the release of ADP from the rear head are therefore left out of the model (the second column from the left in the scheme with four states in grey).[3]

Four more states can be discarded on basis of a similar principle. Because the binding of ATP (to the front head because of the former consideration) results in a tugging force on the rear head, it is energetically unfavorable (thus improbable) for ATP to bind to kinesin before the rear head is detached (in the KD-state). Therefore the transitions from the KT- and KP-state to the TT- and TP-state respectively are disregarded, thereby logically discarding the four states in the lower-right corner of the scheme.

Finally we assume that ATP can only hydrolyze once the deformation of the head associated with its binding has taken place. This assumption effectively discards the transition from the TD-state to the PD-state.

A single state or group of states that does not take part in the motility cycle but has only one connection to it, may act as a "waiting" state, lowering the effective rates to leave the state to which it is attached, see the appendix for details. The PD-state has such properties with respect to the DP-state in the motility cycle, whence we apply this principle there, combining those two states into one.

We now have reduced our model to six states with only seven transitions, as depicted in Fig. 2. There are two main cycles in the model. One runs through the KT-state, the other through the DP-state. Four transitions depend on load, one on the ATP concentration, one on the ADP concentration and one on the concentration of P_i.

3.2. The Rates of the Model

Because on a microscopic level every step should in principle be reversible, every rate in one direction is accompanied by a non-zero rate for the reversed transition: in reality chemical potential differences or loads are not infinite. For the rest, we take the rates of the form (7) satisfying (6) and giving a physical parametrization.

[3] These states occur if ATP concentrations get too low for motility and would effectively be a waiting state with double binding force (KK-state) and some "get-back-to-mobile" states if ATP concentrations become sufficiently high again; it could still play a role at high loads.

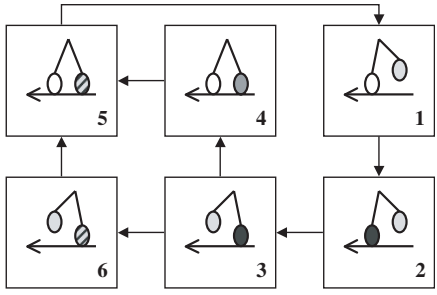

Fig. 2. Scheme of Markov states for our model of kinesin. The arrows indicate the typical direction of the process; the numbers refer to the numbers in the lower right corner of the chemical states in Fig. 1.

As the motor goes through a cyclic process, it eventually returns to each state. Since each state has an associated internal energy, the internal energy difference over every cycle in the model should be zero: $U_{12}+U_{23}+U_{34}+U_{45}+U_{51}=0$, $U_{34}+U_{45}=U_{36}+U_{65}$. Note that this is always true due to the definition of $U_{ij}=G_i-G_j$. In fact here we assume that even $U_{45}=U_{36}$ since one expects the associated reactions to be (almost) independent of the configuration of the other head.

Similarly the motor is displaced by distance λ through a motility cycle. If we assume that transitions involving a reaction from ATP to ADP+P_i or dissociation of P_i do not depend on load we get that $\lambda_{12}+\lambda_{23}+\lambda_{34}=\lambda$ and $\lambda_{65}=\lambda_{34}$. So every one of these transitions account for a bit of movement.

For practical purposes we express the rates belonging to transition (i, j) in terms of concentration of substance α rather than in chemical potentials, writing $\exp(\beta\mu_\alpha)=K_\alpha[\alpha]$. In what follows the energies are expressed in units where $\beta=1$.

The transition from the 1- to the 2-state depends linearly on the ATP concentration, with a coefficient $\omega_{12}K_{ATP}$ that was determined to lie between $1.2-2.8\ \mu M^{-1}s^{-1}$.[14] The increase in the Michealis–Menten constant with load[4, 3] together with the fact that ATP-binding results in a power-stroke,[9] leads us to believe that this transition is also force dependent at some characteristic length λ_{12} and against some internal energy difference U_{12}:

$$r(1,2)=\frac{\omega_{12}K_{ATP}[ATP]}{1+\exp[F\lambda_{12}-U_{12}]} \tag{17}$$

where we use the K_{ATP}, λ_{12} and U_{12} as fitting parameters. For the transition rate in the opposite direction $r(2, 1)$ we use $r(2, 1)(F = 0) = 70\ s^{-1}$ [14] to solve ω_{12}.

The power stroke, where the system goes from the 2-state to the 3-state, is of course also load dependent. We assume that the associated internal energy difference U_{23} lies (well) below 20 kT keeping in mind as a bound that the hydrolysis of one ATP molecule releases a free energy of about 20 kT at room temperature.

For rate $r(2, 3)$ we estimate $\omega_{23} = 10^4\ s^{-1}$; λ_{23} and U_{23} need to be fitted.

Transition (3, 4) may involve some load dependence and we take $r(3, 4)(F = 0) = 306\ s^{-1}$ to fit ω_{34}. In this transition ADP is released from the binding head, so the reverse rate depends on the concentration of ADP:

$$r(4, 3) = K_{ADP}[ADP] \exp[F\lambda_{34} + U_{34}]\, r(3, 4) \tag{18}$$

Transition (4, 5) is simply dissociation of ATP into ADP+P_i, and no dependence on load is expected here. Hence we may simply write $r(4, 5) = \omega_{45}$ and $r(5, 4) = \omega_{45} \exp[-U_{45}]$, where we choose $\omega_{45} = 10^4$. Analogously we write $r(5, 1) = \omega_{51}$ and $r(1, 5) = K_P[P_i] \exp[-U_{51}]$ for the rate-limiting transition, and keep in mind that $r(5, 1)$ should be of the order of $100\ s^{-1}$.[4]

The transitions out of state 6 are special because of the aforementioned reduction of states that has regrouped the DP- and PD-states, see the end of 3.1 and the appendix for details . For the rest, the transitions (3, 6) and (6, 5) are equivalent with transitions (4, 5) and (3, 4), respectively. Looking back at the reduction of states at the end of the appendix, we thus write the rates to *leave* state 6 as

$$r(6, 3) = \frac{r(5, 4)}{1 + \exp[F(\lambda_{12} + \lambda_{23}) - U_{23} + U_{45}]} \tag{19}$$

$$r(6, 5) = \frac{r(3, 4)}{1 + \exp[F(\lambda_{12} + \lambda_{23}) - U_{23} + U_{45}]} \tag{20}$$

Here $\lambda_{12} + \lambda_{23}$ is obviously the distance the head has to move to be in the rearward position, and $U_{23} - U_{45}$ is the energy that is gained by restringing the lever that is associated with the power stroke in the fixed head.

From equilibrium thermodynamics,

$$e^{\beta \Delta\mu} = e^{\beta \Delta G} \frac{[ATP]}{[ADP][P]}, \tag{21}$$

[4] From chemical analysis it is estimated to be only about half of that;[14] optical trap experiments measure however speeds up to 813 nm/s which would be equivalent to a rate of at least $100\ s^{-1}$.

Table I. Relevant Parameters for the Rates Given in Section 3.2 Under Minimization of λ_{12} (Fit 1)

(i, j)	ω_{ij} (s^{-1})	λ_{ij} (nm)	U_{ij} (kT)	α	K_α (M^{-1})
(1, 2)	694	2.55	2.19	ATP	2020
(2, 3)	10^4	5.14	7.91	–	–
(3, 4)	10^4	0.40	−3.45	ADP[a]	2020
(4, 5)	10^4	0	−1.0	–	–
(5, 1)	601	0	−5.64	P_i[a]	$2.1 \cdot 10^{-9}$
(3, 6)	10^4	0	−1.0	–	–
(6, 5)	10^4	0.40	−3.45	ADP[a]	2020

[a] Marks the substances that are *released* in a progressive cycle; $T = 300$ K.

which implies

$$\frac{K_{\mathrm{ATP}}}{K_{\mathrm{ADP}} K_{\mathrm{P}}} = e^{\beta \Delta G} \tag{22}$$

where we take $\Delta G = 20kT$.[10] The exact value of ΔG is not very important for the quality of the results but it plays a role in the thermodynamic prediction of the stall force. We are interested in the regime where the concentrations of ADP and P_i are small. We choose $[\mathrm{ADP}] = [P_i] = 1$ nM and the ATP concentration, together with the load, is the major variable. We also take $K_{\mathrm{ADP}} = K_{\mathrm{ATP}}$ or, from (22), $K_{\mathrm{P}} = \exp(-\beta \Delta G)$. We checked that there was no qualitative dependence of the fitting on small changes in these choices. A summary of the resulting rates is given in Tables I and II.

Table II. Relevant Parameters for the Rates Given in Section 3.2 Under Minimization of ω_{51} (Fit 2)

(i, j)	ω_{ij} (s^{-1})	λ_{ij} (nm)	U_{ij} (kT)	α	K_α (M^{-1})
(1, 2)	2500	3.85	3.51	ATP	500
(2, 3)	10^4	3.74	12.0	–	–
(3, 4)	10^4	0.51	−3.45	ADP[a]	500
(4, 5)	10^4	0	1.95	–	–
(5, 1)	187	0	−14.0	P_i[a]	$2.1 \cdot 10^{-9}$
(3, 6)	10^4	0	1.95	–	–
(6, 5)	10^4	0.51	−3.45	ADP[a]	500

[a] Marks the substances that are *released* in a progressive cycle; $T = 300$ K.

3.3. Fitting of the Model

As is clear from the previous section, the states of the Markov chains have a fixed interpretation and most rates are at least partially determined by the biochemical data but some parameters remain free. The data that we use to fit to, are summarized in Fig. 2 of ref. 3, This fitting consists of the maximal velocity and Michealis–Menten constant at three different forces. That is the main additional input to our model. A fourth measuring point comes from their measurement of the stall force at a cut-off time of 2 seconds: the stall force seems to saturate -at infinite ATP concentrations- to about 8.5 pN. It implies that the velocity cannot exceed $\frac{1}{2}\lambda\ \mathrm{s}^{-1}$. We use $v_{\max}(F = 8.5\ \mathrm{pN}) = \frac{1}{2}\lambda\ \mathrm{s}^{-1}$ as another fitting point.[5] As a consequence we choose not to force the velocity to become strictly zero at a load of about 6–8 pN.

We found it most convenient to start by fitting to the maximal velocities associated with saturating ATP concentrations, since then transition $1 \to 2$ and thus its three parameters K_{ATP}, λ_{12} and U_{12} play no role. Next, we fit the remaining parameters to the values of the Michaelis–Menten constant. Two basic fittings have been obtained, one under minimization of λ_{12} (fit 1) and one under minimization of ω_{51} (fit 2) without allowing U_{23} to become bigger than 12 kT.[6] Experimentally one could distinguish between these extremes by seeing whether there is a maximum in the Michaelis–Menten constant or not beyond 5 pN (see Fig. 9).

The results of these fittings can be seen in Table I and II. Under minimization of λ_{12} (fit 1) ω_{51} becomes fairly big compared to earlier estimates; also U_{23} seems to be rather small in this case and also K_{ATP} seems big. On the other hand it may seem strange that for fit 2 $\lambda_{12} \approx \frac{1}{2}\lambda$. *A priori* we see no good reason to choose either one of these fittings as "the right one." We will continue to refer to them as fit 1 versus fit 2 and they can be considered as two different numerical solutions of the same model.

4. RESULTS

4.1. Velocity

The average velocity of kinesin can be measured as a function of ATP concentration and external load. It is the average distance travelled by the

[5] This will be taken up further in Section 4.2; taking values lower than $\frac{1}{2}\lambda$ increases the fitting error.

[6] Allowing U_{23} to increase even further leads to an unrealistically high free energy difference for transition (5, 1) while on the other hand the results of the next section would remain the same.

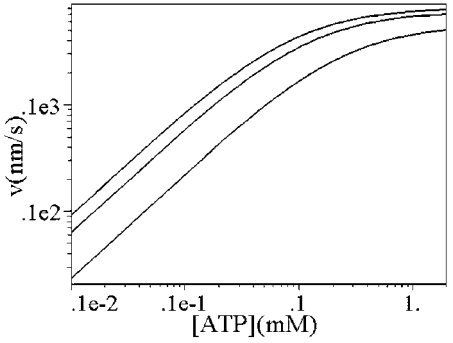

Fig. 3. Logarithmic plot of the velocity as a function of ATP concentration for various loads (from top to bottom 1 pN, 3 pN, and 5 pN).

motor per unit time. In our Markov chain, it is given by the rate at which the system runs the basic cycle $1 \to 2 \to 3 \to 5 \to 1$. Since each cycle is associated with a fixed length λ, we take $\langle v \rangle = \lambda J$ as velocity in our model, with

$$J = J_{51} \equiv r(5, 1)\, \rho(5) - r(1, 5)\, \rho(1) \tag{23}$$

the average (particle) current in the stationary Markov chain between states 5 and 1.

Running our Markov chain gives rise to Figs. 3 and 4 for the behavior of velocity as a function of ATP concentration and load respectively. The

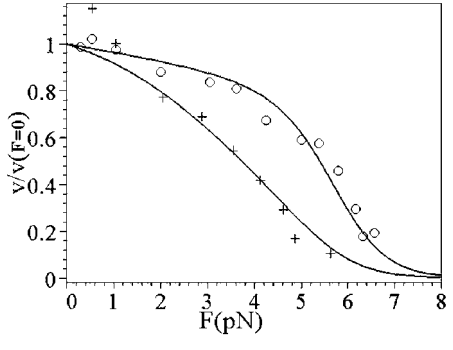

Fig. 4. Normalized plot of the velocity as a function of load for ATP concentrations of 2 mM (top, ○) and 5 μM (bottom, +). The points measured by ref. 3 are indicated in the figure.

relative error with respect to the fitting of ref. 3 remains within 3.5%. For very small loads at [ATP] concentration of 5 μM the agreement is not so good as the fitting obtained in ref. 1. On the other side, for large loads (and this is relevant for the stalling behavior), in contrast with, e.g., ref. 1, our theoretical velocity curve does not vanish at around 7 pN; it decays more slowly and becomes zero when $F\lambda = \Delta\mu$ as corresponds to the thermodynamics of Section 2.1 and Eq. (16). Strictly speaking however, the curve remains in full agreement with the experimental data of ref. 3. Moreover, whereas some theories of kinesin function like[1] even predict that the velocity becomes negative for high loads, the experimental findings of ref. 25 tell that kinesin does not walk back under loads of up to 13 pN.

Turning to analytical results, one expects the velocity $\langle v \rangle = \lambda J$ to qualitatively follow Michaelis–Menten kinetics, that is

$$\langle v \rangle \approx v_{\mathrm{MM}} = \lambda J_{\max} \frac{[\mathrm{ATP}]}{[\mathrm{ATP}] + K_{\mathrm{m}}} \tag{24}$$

where $J_{\max}$ is the maximal current (at saturating ATP concentration) and K_{m} is called the Michaelis–Menten constant, both dependent on the external load.[3] Experimentally (and also in our numerical results), this law is obeyed from near zero loads to at least 5.5 pN with K_{m} increasing with the load. If, in our model, we put $[\mathrm{P_i}] = 0$ (which really corresponds to the case where $[\mathrm{P_i}] \ll [\mathrm{ATP}]$), then $r(1, 5)$ vanishes. We can then calculate the current J with definition (23) and we indeed find the Michaelis–Menten form (24). For this calculation, it suffices to check that the stationary distribution ρ has a very specific form:

$$\rho(1) = \frac{K_{\mathrm{m}}}{[\mathrm{ATP}] + K_{\mathrm{m}}}; \qquad \rho(i) = \frac{\tilde{\rho}(i)[\mathrm{ATP}]}{[\mathrm{ATP}] + K_{\mathrm{m}}}, \tag{25}$$

where $\tilde{\rho}(i)$ are positive numbers that do not depend on the ATP concentration and are given in the appendix. Of course, in reality, $[\mathrm{P_i}] \neq 0$ and $[\mathrm{ADP}] \neq 0$ and this is important when considering small ATP concentrations (near equilibrium situation) as it then happens that the current becomes neagtive for large enough loads. This is not visible in the Michaelis–Menten form (24) and we suggest therefore the modification

$$J = \frac{J_{\max}[\mathrm{ATP}] + J_{\min} K_{\mathrm{m}}}{[\mathrm{ATP}] + K_{\mathrm{m}}} \tag{26}$$

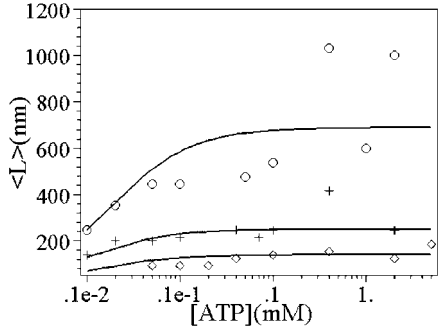

Fig. 5. The mean run length as a function of ATP concentration at various loads, from top to bottom at 1.1 pN (○), 3.6 pN (+) and 5.6 pN (◇); the lines are fittings (see Section 4.5 and Table III), the points are measurements of ref. 4.

where $J_{\min} = \lim_{[\mathrm{ATP}]\downarrow 0} J$ as we verify that $K_{\mathrm{m}} \approx \sum_i \tilde{\rho}(i)\, r(i,1)[\mathrm{ATP}]/r(1,2)$ does not depend on the ATP concentration. This relation (26) will also be important for the stalling behavior of the motor (when $J \approx 0$).

4.2. Stalling the Motor

The external load that is applied to kinesin reaches a certain maximum at the moment kinesin stalls. This maximum force has been referred to as the "stall force" F_{stall}. It has been almost universally recognized that this stall force varies around 5–8 pN. Moreover, the measurements of ref. 3 suggest that the stall force is concave as function of the chemical potential difference. All this looks like being in contradiction with the thermodynamics of Section 2.3 where, around (15), we found from considerations on

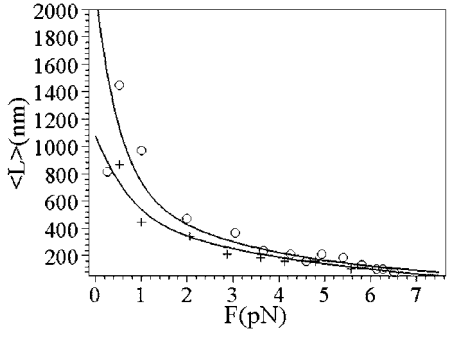

Fig. 6. The mean run length as a function of load at high ATP concentrations (○ = 2 mM) and low ATP concentrations (+ = 5 μM); the lines are fittings (see Section 4.5 and Table III), the points are measurements of ref. 4.

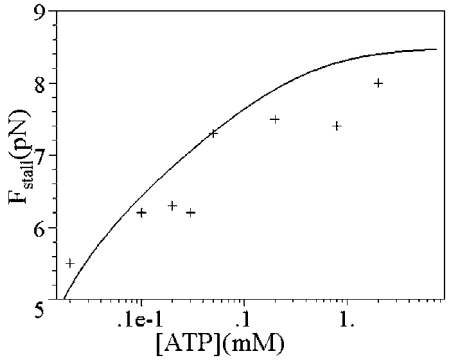

Fig. 7. The experimental stall force measured by ref. 4 (+) compared with the line of equal velocity for fit 1; the solution of $\langle v \rangle = \frac{1}{2}\lambda$. As can be seen this line at least roughly represents the measurements.

the mean entropy production that $\lambda F_{st} = \Delta\mu$. This contradiction can be removed by being more clear about the nature of stalling, as we will now explain.

In order to measure the stall force in an experimental set-up, one has to choose a certain finite cut-off time τ during which the motor should not move; from that time the motor is considered to have stalled.[7] Doing measurements on the stall force using such a cut-off time τ as a function of the parameters comes down to an integration over the variable velocity $v(t)$ seeing that it remains within some error interval, say $\int_0^\tau v(t)\,dt < \delta$. The apparent contradiction above disappears if we assume that the stalling condition is equivalent with solving the equation $v([\mathrm{ATP}], F) = \lambda/\tau$ for reasonable τ. After all, experimentally the stall regime is identified as a horizontal plateau in displacement records and the plateau duration is not infinite. In Fig. 7 we have connected the points where the force and the concentration give the velocity $\langle v \rangle = \frac{1}{2}\lambda$ for fit 1; this should be compared with Fig. 3b in ref. 3. As is clear, this profile resembles the experimental stall force, in support of our assumption.

Because we have the velocity rather explicitly in terms of the ATP concentration, (26), we solve the equation $v([\mathrm{ATP}], F) = \lambda/\tau$ in terms of [ATP], obtaining the stall concentration

$$[\mathrm{ATP}]_{st}(\tau) = \frac{K_m(\frac{1}{\tau} - J_{min})}{J_{max} - \frac{1}{\tau}} \tag{27}$$

[7] There is an experimental consideration to be made for the statistical evaluation of the stall force: in a considerable fraction of runs, for not too small loads, the motor dissociates before stalling which could lead to a biased sampling at high loads, see also ref. 25.

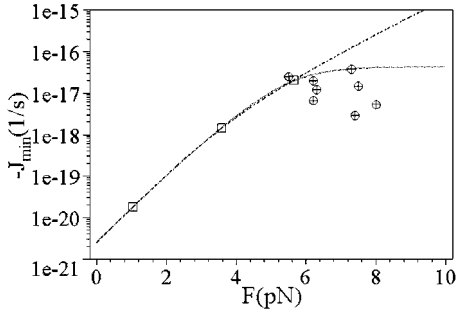

Fig. 8. Logarithmic plot of $-J_{\min}$. The two lines indicate the direct calculation of our model using two different fittings ("$\cdots$" for fit 1, "$-\cdot-$" for fit 2), the three points to the left are calculations using the parameters of the Michaelis–Menten fit of ref. 3 (□'s using (28)) the points to the right are calculations using their measurement of the stall load (○'s and +'s for fit 1 and 2 respectively using (27) with $\tau = 2$ s).

Hence, for some finite load and some finite τ the stall concentration can be infinite. This is again consistent with the findings of ref. 3, their Fig. 3b.

We can also use the Eq. (27) to obtain numerically the load dependence of $J_{\min}$ and K_m. In Fig. 8 the results can be seen on the measurements of ref. 3. For small loads fit 1 follows the experimental values perfectly and for larger loads fit 1 seems to have better characteristics compared to fit 2 as well, even though many of the experimental points are scattered towards lower values. Of course, also K_m is load dependent. In Fig. 9 we see the

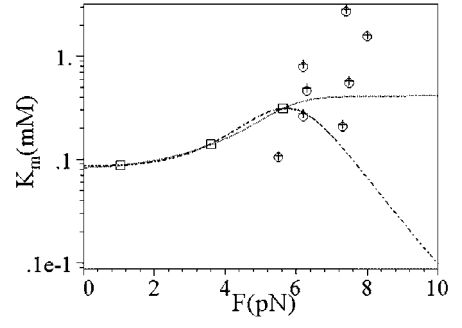

Fig. 9. The two lines indicate the direct calculations of K_m from our model using two different fittings ("$\cdots$" for fit 1, "$-\cdot-$" for fit 2), the three points to the left are calculations using the parameters of the Michaelis–Menten fit of ref. 3 (□'s), the points on the right are calculations using their measurement of the stall load (∘'s and +'s for fit 1 and 2 respectively). The best fitting would seem to be fit 1 with respect to the characteristics. Unfortunately the points on the right seem too widely scattered to draw strong conclusions.

results of calculating K_m from the measurements of the stall load of ref. 3. K_m is certainly of the right order, but the points are rather wide-spread. When compared with our model, fit 1 seems to do better than fit 2 here just as well.

Equation (27) also gives a new interpretation to the term J_{min} that first appeared in (26): it is proportional to the finite stall concentration when stalling is defined with infinite waiting time τ (plateau duration),

$$\lim_{\tau \to \infty} [\mathrm{ATP}]_{st}(\tau) = [\mathrm{ATP}]_{st} \Rightarrow J_{min} = -\frac{J_{max}}{K_m}[\mathrm{ATP}]_{st} \tag{28}$$

4.3. Entropy Production

As can be seen from the general discussion around (2), the total steady state entropy production $Q + (\mu_1 - e_1) - (\mu_2 - e_2) \geqslant 0$ consists of two contributions: there is the heat Q given to the body and there is the deterioration of the energy source (hydrolysis of ATP). For fixed concentrations, the waste (even though pleasant) is just in the heating.

It is quite straightforward to calculate the mean entropy production for our model with Eq. (10). As one expects, the outcome increases with ATP concentration and it decreases with load. Increasing the load decreases the velocity but increases the work per particle $W = F\lambda$. Since energy conservation (1) implies that for greater work W, less heat per particle Q can be dissipated and hence the heat current QJ decreases, it is indeed as expected that the entropy production rate decreases with increasing load.

It is interesting to calculate the mean entropy produced per ATP molecule. To do so we divide the mean entropy production by the ATP consumption, which is the same as the current J (26) since only one ATP molecule is used per cycle. We have numerically calculated that the entropy production per cycle is linear with log[ATP] and with load, the slopes are 1 and $-\beta\lambda$ respectively. This is in full correspondence with (2). In case the motor does no work, $W = F\lambda = 0$, we expect $\beta \Delta\mu = \mathrm{MEP}/J$; $\beta \Delta\mu = \beta \Delta G + \log[\mathrm{ATP}] - \log[\mathrm{ADP}][\mathrm{P_i}] \approx 55$ for $[\mathrm{ATP}] = 2$ mM. We find that fit 1 and fit 2 both give results in full correspondence with theory.

4.4. Efficiency

Estimating efficiencies for molecular motors is still an issue of debate. In ref. 26 it is argued that one should not only consider the power for motion but also to do this with a given average velocity, thereby, e.g., taking into account that the motor moves in a viscous medium. As it is the case even for chemical plants, the proper definition of efficiency surely depends on what you wish to keep constant and what is considered as

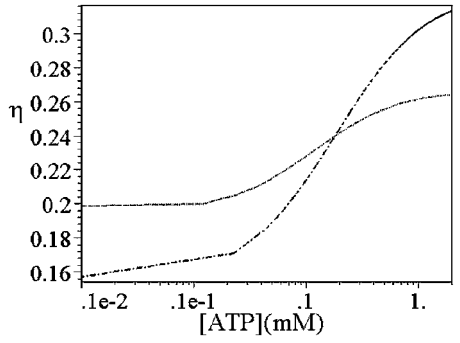

Fig. 10. Semi-logarithmic plot of η as a function of [ATP] for $F = 3.2$ ($\cdots$) and $F = 4.5$ pN ($- \cdot -$), belonging to the maxima of the curves in Fig. 11. Obviously the maximal efficiency increases with [ATP], but for extremely large [ATP] it decreases again (not shown in plot).

waste. Here we take the conventional set-up that centers around the question what force is exerted by a molecular motor to keep moving, see ref. 18.

An efficiency usually counts the actual work performed by the motor divided by the maximal possible work (input energy). We will speak in terms of power output versus power input. The numerator, the power output, is easy: it is just $JF\lambda$. For the denominator, which is always more problematic, we can follow the standard thermodynamics that we had before. From (3), we have the bound on the work $W \leqslant \mu_1 - \mu_2$ so that the maximal input power is $\Delta\mu$ multiplied with the maximum current $J_0 = J(F = 0)$. The denominator is thus taken equal to $J_0 \Delta\mu$, the chemical potential current without load, and does not depend on the load. We thus have as "efficiency:"

$$\eta = \frac{JF\lambda}{J_0\, \Delta\mu} \tag{29}$$

The behavior of this "efficiency" for our model can be seen in Figs. 10 and 11. As expected it has a maximum as a function of load and it increases with ATP concentration in the experimental regime. There seems to be a global maximum of about 32% at an ATP concentration of approximately $9 \cdot 10^{-2}$ M and a load of about 4.6 pN.

4.5. Mean Run Length

The processivity of kinesin along the microtubular track refers to the attachment of the motor. The average distance travelled before detachment of the motor from the microtubule $\langle L \rangle$ was experimentally measured by

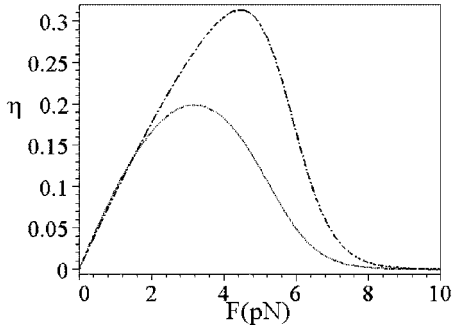

Fig. 11. Plot of η as a function of load for $[ATP]=10^{-6}$ $(\cdots)$ and $[ATP]=2\cdot10^{-3}$ M $(-\cdot-)$. This efficiency clearly has a maximum at some specific load that increases with [ATP] from approximately 3.2 pN for $[ATP]=10^{-6}$ to about 4.5 pN for $[ATP]=2\cdot10^{-3}$ M.

ref. 4. It depends on the average velocity $\langle v\rangle$ and the rate of detachment r_{det} in the following way:

$$\langle L\rangle = \frac{\langle v\rangle}{r_{\text{det}}} \tag{30}$$

The velocity has been treated in Section 4.1, remains the rate of detachment.

The rate of detachment for our model is the sum over all possible ways to detach, summing over all rates of detachment from a specific state, weighted with the probability to be in that state:

$$r_{\text{det}} = \sum_i \rho(i)\, r_{\text{det}}(i) \tag{31}$$

A first natural candidate where the detachment rate is non-zero is the PD-state. The PD-state was taken in our model as part of the 6 state and the corresponding rate of detachment would be according to Eqs. (7), (19), and (20) and the considerations made at the end of the appendix:

$$\rho(\text{PD})\, r_{\text{det}}(\text{PD}) = \frac{\rho(6)}{1+e^{U_{23}-U_{45}-F(\lambda_{12}+\lambda_{23})}} \frac{\omega_{6,\,\text{det}}}{1+e^{U_{6,\,\text{det}}-F\lambda_{6,\,\text{det}}}} \tag{32}$$

where the first part determines the PD-state part of the probability distribution of state 6 and the second part is the actual detachment rate containing some fitting parameters $\omega_{6,\,\text{det}}$, $U_{6,\,\text{det}}$, and $\lambda_{6,\,\text{det}}$. Moreover, the experimental data indicate that the average distance travelled decreases

Table III. Fitting Parameters for the Detachment Rates Given in Section 4.5

(i, j)	ω_{ij} (s^{-1})	λ_{ij} (nm)	U_{ij} (kT)
(1, det)	$2.4 \cdot 10^{-2}$	4.1	5.0
(6, det)	$4.8 \cdot 10^{4}$	6.9	0.7

with decreasing ATP concentrations,[4] suggesting that detachment may occur in the KD-state (state 1) prior to binding with an ATP molecule.[8] The corresponding detachment rate for state 1 would be:

$$\rho(1)\, r_{\text{det}}(1) = \frac{\omega_{1,\text{det}}}{1 + e^{U_{1,\text{det}} - F\lambda_{1,\text{det}}}} \tag{33}$$

introducing another three fitting parameters $\omega_{1,\text{det}}$, $U_{1,\text{det}}$, and $\lambda_{1,\text{det}}$. Since we expect that the binding of the KD-state is a bit more stiff than that of the DP-state, $U_{1,\text{det}}$ should be larger than $U_{6,\text{det}}$ on the one hand and $\lambda_{1,\text{det}}$ should be smaller than $\lambda_{6,\text{det}}$ on the other hand.

In Figs. 5 and 6 the results of this approach are given, where we have used values for the fitting parameters as stated in Table III (fit 1 and 2 are compatible here). With the fitting of the additional parameters, the processivity behavior is well reproduced.

5. CONCLUSIONS

Our purpose was not to find a simple model with parameters that would fit sufficiently well the experimental data concerning kinesin. An essential part of our results is in the very construction of the Markov model, rather independent of the experimental processivity data but inspired by and based on the mechanochemical structure of the motor (for the Markov states) and on the observed transitions (for the rates). We have then found *a posteriori* that the velocity and stalling data and their dependence on load and ATP concentrated are well reproduced. Furthermore, we have connected the motor functioning with thermodynamics and have investigated how the entropy production and the efficiency depend on load and ATP concentration. The theory of fluctuations of the entropy production and the associated randomness in the motion has not yet been explored here.

[8] That makes sense since it is the first state in our model that is reached when a kinesin molecule binds to the microtubule *from* a detached state.

APPENDIX

To obtain a Markov chain on a smaller state space from whose stationary state we can however reconstruct the original stationary solution, the following result is helpful.

We write $\Omega = \{1, 2,..., n\}$ and we suppose that all states are connected via some path of strictly positive transition rates $r(i, j) > 0$ (we can of course always put $r(i, i) = 0$).

The stationary probability distribution can be written as:

$$\rho(1) = \frac{\sum_{j=2}^{n} \tilde{\rho}(j)\, r(j, 1)}{\sum_{j=2}^{n} [\tilde{\rho}(j)\, r(j, 1) + r(1, j)]}; \qquad \rho(j) = \tilde{\rho}(j)(1 - \rho(1)), \quad j \neq 1 \tag{34}$$

with $\tilde{\rho}$ a probability measure on $\{2,..., n\}$ which is the solution of

$$\sum_{j=2}^{n} [\tilde{\rho}(i)\, \tilde{r}(i, j) - \tilde{\rho}(j)\, \tilde{r}(j, i)] = 0, \qquad \forall i \neq 1 \tag{35}$$

where

$$\tilde{r}(i, j) \equiv C \left[r(i, j) + \frac{r(i, 1)\, r(1, j)}{\sum_l r(1, l)} \right], \qquad i, j \in \{2,..., n\}. \tag{36}$$

where C is an arbitrary positive constant (a rescaling of time).

Note that we can again set $\tilde{r}(i, i) = 0$ and

$$\sum_{j=2}^{n} \tilde{r}(i, j) = C \sum_{j=1}^{n} r(i, j), \qquad i \in \Omega \setminus \{1\} \tag{37}$$

These new rates $\tilde{r}(i, j)$ are the rates for a reduced Markov chain on the reduced state space $\Omega \setminus \{1\}$.

Proof. The stationarity of $\rho(1)$ can be rewritten from Eq. (9) as

$$\rho(1) \left[(1 - \rho(1)) \sum_j r(1, j) + \sum_j \rho(j)\, r(j, 1) \right] = \sum_j \rho(j)\, r(j, 1) \tag{38}$$

from which we get $\rho(1)$ as function of the $\tilde{\rho}(j)$'s as in (34); The $\tilde{\rho}(j)$'s are a rescaling of the original $\rho(j)$'s, and they sum up to one. They are also the stationary solution of a new Markov chain, because we can rewrite (9) for the other states ($i \neq 1$):

$$\rho(i) \left[\sum_{j \neq 1} r(i, j) + r(i, 1) \right] = \sum_{j \neq 1} \rho(j)\, r(j, i) + \rho(1)\, r(1, i) \tag{39}$$

Upon dividing this by $1-\rho(1)$ and by substituting (34), we find the Eq. (35). ▮

Another type of reduction of states is useful when there is a state which is connected to only one other state. We consider then the Markov chain with $r(1, i) = 0 = r(i, 1)$ unless $i = 2$. Let again ρ denote the unique stationary probability distribution and define $\hat{\rho}(i) = \rho(i)$ for $i = 3,\ldots, n$ and $\hat{\rho}(2) = \rho(1) + \rho(2)$ for a new probability measure on $\Omega \setminus \{1\}$. Then, $\hat{\rho}$ is stationary for the (new) Markov chain with transition rates $\hat{r}(i, j) = r(i, j)$ if $i \neq 2$ and $\hat{r}(2, j) = r(2, j)[1 + r(2, 1)/r(1, 2)]^{-1}$.

The proof of this last reduction starts by observing that in the original Markov chain $J_{12} = 0$, i.e., $\rho(1)\, r(1, 2) = r(2, 1)\, \rho(2)$, which just expresses the stationarity for $i = 1$ in (9). The rest is just explicitly checking the stationarity of $\hat{\rho}$ under the transition rates $\hat{r}(i, j)$ while using that $r(i, 1) = r(1, i) = 0$ for $i \neq 2$ and that $\hat{r}(2, j)\, \hat{\rho}(2) = \rho(2)\, r(2, j)$.

ACKNOWLEDGMENTS

We are grateful to Karel Netočný and Frank Redig for many discussions.

REFERENCES

1. M. E. Fisher and A. B. Kolomeisky, *Proc. Nat. Ac. Sc.* **98**:7748 (2001).
2. A. Mogilner, A. J. Fisher, and R. J. Baskin, *J. Theor. Biol.* **211**:143–157 (2001).
3. K. Visscher, M. J. Schnitzer, and S. M. Block, *Nature* **400**:184 (1999).
4. M. J. Schnitzer, K. Visscher, and S. M. Block, *Nature Cell B* **2**:718 (2000).
5. C. Maes and K. Netočný, *J. Stat. Phys.* **110**, 269–310 (2003).
6. G. M. Wang, E. M. Sevick, and E. Mittag, *et al.*, *Phys. Rev. Lett.* **89**:050601 (2002).
7. T. L. Hill, *Thermodynamics of Small Systems* (Dover 2002).
8. R. D. Vale and R. A. Milligan, *Science* **288**:88 (2000).
9. S. Rice, A. W. Lin, and D. Safer, *et al.*, *Nature* **402**:778 (1999).
10. J. Howard, *Mechanics of Motor Proteins and the Cytoskeleton* (Sinauer, 2001), p. 231.
11. M. J. Schnitzer and S. M. Block, *Nature* **388**:386 (1997).
12. W. Hua, E. C. Young, M. L. Flemming, and J. Gelles, *Nature* **388**:390 (1997).
13. W. Hua, J. Chung, and J. Gelles, *Science* **295**:844 (2002).
14. M. L Moyer, S. P. Gilbert, and K. A. Johnson, *Biochemistry* **37**:800 (1998).
15. Hong Qian, *J. Math. Chem.* **27**:219–234 (2000).
16. P. Reimann, *Phys. Rep.* **361**:57 (2002).
17. F. Jülicher, A. Ajdari, and J. Prost, *Rev. Mod. Phys.* **69**:1269 (1997).
18. M. E. Fisher and A. B. Kolomeisky, *Proc. Nat. Ac. Sc.* **96**:6597 (1999).
19. C. S. Peskin and G. Oster, *Biophys. J.* **68**:202s (1995).
20. M. A. Leontovich, *J. Experiment. Theoret. Phys.* **5**:211 (1935).
21. D. A. McQuarrie, *J. Appl. Prob.* **4**:413 (1967).

22. C. Maes, F. Redig, and A. Van Moffaert, *J. Math. Phys.* **41**:1528 (2000).
23. J. Schnakenberg, *Rev. Mod. Phys.* **48**:571 (1976)
24. L. Romberg and R. D. Vale, *Nature* **361**:168 (1993).
25. C. M. Coppin, D. Pierce, L. Hsu, and R. D. Vale, *Proc. Nat. Ac. Sc.* **94**:8539 (1997).
26. I. Derényi, M. Bier, and R. D. Astumian, *Phys. Rev. Lett.* **83**:903 (1999).